Gradient calculation for anisotropic FWI

Junxiao Li, Wenyong Pan, Kristopher A. Innanen and Guo Tao

ABSTRACT

The 3-D TTI medium can be characterized as eight parameters (5 independent elastic moduli in constitutive coordinate system, density, tilt as well as azimuth angle) at each spatial point. One of the key issues in implementing FWI for parameter characterizing TTI media is efficient gradient calculation of objective function with respect to each model parameter. To calculate the gradient of each independent parameter involves the synthetic and adjoint data, as well as the derivatives of elastic moduli with respect to the independent parameters of the model. In this paper, the synthetic and adjoint wavefields are simulated with a staggered-grid finite-difference algorithm in anisotropic media. The derivatives of the elastic modulus tensor for TTI media are also analyzed in this paper. Numerical examples of the gradients calculation are thus illustrated in a three-layer TTI model. One of the issues addressed in the discussion is that the synthetic data at each time step should be stored on the disk so as to perform cross-correlation with the adjoint wavefields to generate the gradient for FWI in time domian. The huge dataset storage during synthetic wavefield simulation and loading when calculating the gradient is highly memory cost and time consuming. The use of random boundary layer allows us to compute both the adjoint and synthetic wavefield simultaneously without the necessity of storing total synthetic data. In this paper, cubic grains are implemented as random boundary layers. The randomized elastic moduli instead of velocities are thus added in elastic wave equations in TTI medium. The synthetic waveforms with random boundary layers are finally illustrated.

INTRODUCTION

According to (Thomsen, 1986), shale, laminated thin-layers and oriented vertical fractures are transversely isotropic (TI) media. Consistently weathering tectonic movement, fold and overthrusting, the symmetry axis of TI media instead of being either be vertical or horizontal, will have an angle with respect to the observation coordinates system, which is called tilted transversely isotropic (TTI) media. The parameter characterization of TTI media using elastic moduli, tilt angle, polar angle as well as density is of great importance.

Seismic full-waveform inversion (FWI)(Tarantola, 1984; Gauthier, 1986; Mora, 1987; Palloff and Pratt, 1999) is capable of providing formation parameters with high spatial resolution. Over the past few decades, space and time domain FWI (Kolb et al., 1986; Mora, 1987; Bunks et al., 1995) has been paid an increasing interest since the initial work proposed by Lailly (1983) and Tarantola (1984). The recent development of FWI in elastic and anisotropic media (Lee et al., 2010; Kamath et al., 2013) makes it possible for the use of multicomponent reflection data. The gradient of a misfit function can be obtained based on two numerical simulations (forward simulation for current model and time-reversed simulation for adjoint source)(Tromp et al., 2005). Liu and Tromp (2006) derived the gradients of the objective function for an elastic earth model. Lee et al. (2010) performed elastic FWI of synthetic multicomponent seismic data for VTI media with respect to elastic moduli. Kamath et al. (2013) calculated gradients of Thomsen parameters for 2D laterally

heterogeneous VTI media.

On the other hand, recent development of high-performance computing and numerical simulation techniques have made it possible for three-dimensional (3D) simulations of elastic wave propagation in complicated media (Komatitsch and Tromp, 2002). The conventional method of gradient calculation in time domain needs to record synthetic wavefield at each time step to correlate with the adjoint wavefield time reversely, which is highy memory cost. And the shabby input/output (I/O) of recorded data dramatically increases the total running time of the algorithm, which impedes the computational efficiency. Nguyen and McMechan (2014) discussed 5 alternative algorithms avoid storing source wavefield snapshots during forward and backward wavefield correlation in reverse time migration (RTM). Symes (2007) and Anderson et al. (2012) used an optimal checkpointing algorithm to minimize the total storage at the cost of increasing the computational complexity of the adjoint wavefield simulation. Clapp (Clapp, 2008) suggested implementing a boundary re-injection scheme that the wavefield at each time step is saved at the edge of damping zone so as to regenerate the wavefield. Clapp et al. (2009) proposes an alternate random boundary condition method that uses an increasingly random velocity region by replacing the conventional damped region.

In this paper, We first discuss the FWI scheme formulated in the time domain for a 3-D elastic medium. The relationship between elastic moduli in constitutive coordinate system and in 3D TTI medium are then given a detailed review, based on which, the gradients for elastic moduli as well as Thomsen parameters in TTI medium are thus obtained. A three-layer heterogeneous TTI media model is used for gradient calculation with respect to both elastic moduli and Thomsen parameters. Because of the huge dataset storage during synthetic wavefield simulation and loading when calculating the gradient, which is highly memory cost and time consuming, we suggest useing random boundary layer to compute both the adjoint and synthetic wavefield simultaneously without the necessity of storing total synthetic data. During synthetic model simulation, cubic grains are implemented as random boundary layers in this paper. The randomized elastic moduli instead of velocities are thus added in elastic wave equations in TTI medium. The synthetic waveforms with random boundary layers are finally illustrated.

THEORETICAL BACKGROUND

FWI in time domain

For three-component data d_{obs} recorded at N receiver stations, we have the corresponding synthetic data d_{syn}, the aim of time-domain FWI is to find a model $\boldsymbol{m}^*$ minimize the least-squares waveform misfit function:

$$\chi = \frac{1}{2}\sum_{r=1}^{N}\int_0^T \parallel d_{syn} - d_{obs} \parallel^2 dt. \tag{1}$$

Suppose the current model used for the synthetic data is M-dimensional vector $\boldsymbol{m}$, the perturbation in the model that causes the differences between the data and synthetics can

be expressed as

$$\Delta \boldsymbol{m} = -\alpha \left(\frac{\partial \chi}{\partial \boldsymbol{m}} \right), \tag{2}$$

where $\left(\frac{\partial \chi}{\partial \boldsymbol{m}}\right)$ is the gradient direction of the objective function; α is a step length that can be calculated with a linear assumption (Crase et al., 1990):

$$\alpha = \varepsilon \frac{(d_{pert} - d_{syn})^T (d_{syn} - d_{obs})}{(d_{pert} - d_{syn})^T (d_{pert} - d_{syn})}, \tag{3}$$

where d_{pert} is data generated by a small known model perturbation ε.

The iteration of model parameters to minimize χ is thus expressed as

$$\boldsymbol{m}^{n+1} = \boldsymbol{m}^n + \Delta \boldsymbol{m}, \tag{4}$$

where, the superscript n denotes the n^{th} iteration.

According to the above equation, to determine the model update is to compute the gradient of the objective function $\left(\frac{\partial \chi}{\partial \boldsymbol{m}}\right)$. Given a general anisotropic model ρ, c_{ijkl}, in which ρ is the model density and c_{ijkl} is the elastic moduli, according to Liu and Tromp (2006), the $Fréchet$ derivatives with respect to density and the elastic moduli are the 3-D waveform misfit kernels K_ρ and $K_{c_{ijkl}}$ that can be defined as

$$K_{c_{ijkl}} = -\sum_{s=1}^{S} \sum_{r=1}^{R} \int \frac{\partial \delta u_i}{\partial x_j} \frac{\partial G_k}{\partial x_l} dt, \tag{5}$$

in which, u and G are the forward and adjoint displacement wavefields. The gradient of each model parameter m_n can be obtained by chain rule as

$$K_{m_n} = -\sum_{ijkl} K_{ijkl} \frac{\partial c_{ijkl}}{\partial m_n} dt. \tag{6}$$

3-D TTI Medium

According to Thomsen(Thomsen, 1986), the parameters that characterize wave propagation in transversely isotropic medium (TI medium) are

$$V_{P0} = sqrt(\tfrac{c_{33}}{\rho}), \quad V_{P0} = sqrt(\tfrac{c_{55}}{\rho}),$$

$$\varepsilon = \tfrac{c_{11}-c_{33}}{2c_{33}}, \quad \gamma = \tfrac{c_{66}-c_{44}}{2c_{44}}, \quad \delta^* = \tfrac{1}{2c_{33}^2}\left[2(c_{13}+c_{44})^2 - (c_{33}-c_{44})(c_{11}+c_{33}-2c_{44})\right], \tag{7}$$

where Thomsen parameters V_{P0},V_{S0} are phase velocities of qP- and qS- wave along axis of symmetry; ε, γ are degree of qP-, qS- wave anisotropy, $\delta^*$is related to wavefront ellipticity.

In vertical transverse isotropy (VTI) medium, The elastic moduli can also be described by Thomsen parameters as

$$\begin{aligned} c_{11} &= \rho(1+2\varepsilon)V_{P0}^2, \\ c_{13} &= \rho\{V_{P0}^4\delta^* + (V_{P0}^2 - V_{S0}^2)\left[V_{P0}^2(1+\varepsilon) - V_{S0}^2\right]\}^{1/2} - \rho V_{S0}^2, \\ c_{33} &= \rho V_{P0}^2, \\ c_{44} &= \rho V_{S0}^2, \\ c_{66} &= \rho(1+2\gamma)V_{S0}^2. \end{aligned} \tag{8}$$

When there is an angle between the observation coordinate system and axis of symmetry for VTI media, tilted transversely isotropic (TTI) media are generated. Generally, the 3-D TTI medium can be characterized as eight parameters at each spatial point $m_v = \{c_{11}, c_{13}, c_{33}, c_{44}, c_{66}, \rho, \theta, \varphi\}$, in which $c_{11}, c_{13}, c_{33}, c_{44}, c_{66}$ are independent elastic moduli in VTI media in constitutive coordinate system ($[x, y, z]$); θ, φ are the spherical tilt angle and azimuthal phase angle. The auxiliary Cartesian coordinate system $[x', y', z']$ can thus be rotated by the tilt angle θ around z axis (Tsvankin, 2012).

Let's suppose the symmetry axis of TTI media lies in X'OZ' plane in this paper. Based on Bond's law (Winterstein, 1990; Bansal and Sen, 2008; Zhu and Dorman, 2000), the relationship between the elastic moduli matrix $\boldsymbol{C'}$ of TTI medium and the matrix $\boldsymbol{C}$ in VTI is

$$\boldsymbol{C'} = \boldsymbol{R}\boldsymbol{C}\boldsymbol{R}^T, \tag{9}$$

where the Bond transform matrix $\boldsymbol{R}$ is

$$\boldsymbol{R} = \begin{bmatrix} \alpha_1^2 & \beta_1^2 & \gamma_1^2 & 2\beta_1\gamma_1 & 2\alpha_1\gamma_1 & 2\alpha_1\beta_1 \\ \alpha_2^2 & \beta_2^2 & \gamma_2^2 & 2\beta_2\gamma_2 & 2\alpha_2\gamma_2 & 2\alpha_1\beta_1 \\ \alpha_3^2 & \beta_3^2 & \gamma_3^2 & 2\beta_3\gamma_3 & 2\alpha_3\gamma_3 & 2\alpha_1\beta_1 \\ \alpha_2\alpha_3 & \beta_2\beta_3 & \gamma_2\gamma_3 & \beta_2\gamma_3 + \beta_3\gamma_2 & \gamma_2\alpha_3 + \gamma_3\alpha_2 & \alpha_2\beta_3 + \alpha_3\beta_2 \\ \alpha_1\alpha_3 & \beta_1\beta_3 & \gamma_1\gamma_2 & \beta_1\gamma_3 + \beta_3\gamma_1 & \gamma_1\alpha_3 + \gamma_3\alpha_1 & \alpha_1\beta_3 + \alpha_3\beta_1 \\ \alpha_1\alpha_2 & \beta_1\beta_2 & \gamma_1\gamma_2 & \beta_1\gamma_2 + \beta_2\gamma_1 & \gamma_1\alpha_2 + \gamma_2\alpha_1 & \alpha_1\beta_2 + \alpha_2\beta_1 \end{bmatrix}, \tag{10}$$

in which, α, β, γ are the direction cosine of coordinates transform, that satisfy

Table 1. The direction cosine of coordinates transform

	x	y	z
x'	α_1	β_1	γ_1
y'	α_2	β_2	γ_2
z'	α_3	β_3	γ_3

Set azimuthal angle $\varphi = 0$, Bond's matrix in equation (10) (when rotating around the y-axis) is

$$\boldsymbol{R} = \begin{bmatrix} cos^2\theta & 0 & sin^2\theta & 0 & -sin(2\theta) & 0 \\ 0 & 1 & 0 & 0 & 0 & 0 \\ sin^2\theta & 0 & cos^2\theta & 0 & sin(2\theta) & 0 \\ 0 & 0 & 0 & cos\theta & 0 & sin\theta \\ sin\theta cos\theta & 0 & -sin\theta cos\theta & 0 & cos(2\theta) & 0 \\ 0 & 0 & 0 & -sin\theta & 0 & cos\theta \end{bmatrix}. \tag{11}$$

The matrix $\boldsymbol{C}$ in the VTI medium is as follows

$$\boldsymbol{C} = \begin{bmatrix} c_{11} & c_{11}-2c_{66} & c_{13} & 0 & 0 & 0 \\ c_{11}-2c_{66} & c_{11} & c_{13} & 0 & 0 & 0 \\ c_{13} & c_{13} & c_{33} & 0 & 0 & 0 \\ 0 & 0 & 0 & c_{44} & 0 & 0 \\ 0 & 0 & 0 & 0 & c_{44} & 0 \\ 0 & 0 & 0 & 0 & 0 & c_{66} \end{bmatrix}. \tag{12}$$

The matrix $\boldsymbol{C'}$ in the TTI medium is thus obtained according to equations (10) to (12) as

$$\boldsymbol{C'} = \begin{bmatrix} c'_{11} & c'_{12} & c'_{13} & 0 & c'_{15} & 0 \\ c'_{21} & c'_{22} & c'_{23} & 0 & c'_{25} & 0 \\ c'_{31} & c'_{32} & c'_{33} & 0 & c'_{35} & 0 \\ 0 & 0 & 0 & c'_{44} & 0 & c'_{46} \\ c'_{51} & c'_{52} & c'_{53} & 0 & c'_{55} & 0 \\ 0 & 0 & 0 & c'_{64} & 0 & c'_{66} \end{bmatrix}. \tag{13}$$

The above thirteen non-zero elastic moduli in TTI medium can be expressed by the tilt angle and the elastic moduli in VTI medium in constitutive coordinate system as

$$
\begin{aligned}
c'_{11} &= c_{11}cos^4\theta + c_{33}sin^4\theta + 2c_{13})sin^2\theta cos^2\theta + c_{44}sin^2(2\theta),\\
c'_{12} &= c'_{21} = c_{12}cos^2\theta + c_{13}sin^2\theta,\\
c'_{13} &= c'_{31} = c_{13}(cos^4\theta + sin^4\theta) + (c_{11} + c_{33})sin^2\theta cos^2\theta - c_{44}sin^2(2\theta),\\
c'_{15} &= c'_{51} = [(c_{11} - c_{13})\, cos^2\theta + (c_{13} - c_{33})sin^2\theta]\, sin\theta cos\theta - c_{44}sin(2\theta)cos(2\theta),\\
c'_{22} &= c_{11},\\
c'_{23} &= c'_{32} = c_{12}sin^2\theta + c_{13}cos^2\theta,\\
c'_{25} &= c'_{52} = (c_{12} - c_{13})sin\theta cos\theta,\\
c'_{33} &= c_{11}sin^4\theta + c_{33}cos^4\theta + 2c_{13}sin^2\theta cos^2\theta + c_{44}sin^2(2\theta),\\
c'_{35} &= c'_{53} = [(c_{11} - c_{13})\, sin^2\theta + (c_{13} - c_{33})cos^2\theta]\, sin\theta cos\theta + c_{44}sin(2\theta)cos(2\theta),\\
c'_{44} &= c_{44}cos^{\theta} + c_{66}sin^2\theta,\\
c'_{46} &= c'_{64} = (c_{66} - c_{44})sin\theta cos\theta,\\
c'_{55} &= (c_{11} - 2c_{13} + c_{33})sin^2\theta cos^2\theta + c_{44}cos^2(2\theta),\\
c'_{66} &= c_{44}sin^2\theta + c_{66}cos^2\theta.
\end{aligned}
\tag{14}
$$

Gradients for elastic moduli in TTI Medium

As is discussed in last section, the 3-D TTI medium can be characterized as eight parameters at each spatial point $m_v = \{c_{11}, c_{13}, c_{33}, c_{44}, c_{66}, \rho, \theta, \varphi\}$. Based on equation (5) and equation (6), in 3D polar TTI media ($\varphi = 0$), considering a constant density ρ, the gradients of 6 other TTI parameters are expressed as

$$
\begin{aligned}
K_{c_{11}} &= -\sum_{s=1}^{S}\sum_{r=1}^{R}\int\sum_{ijkl}\frac{\partial u_i}{\partial x_j}\frac{\partial G_k}{\partial x_l}\frac{\partial c_{ijkl}}{\partial c_{11}}dt = -\sum_{s=1}^{S}\sum_{r=1}^{R}\int\frac{\partial M_{11}}{\partial c_{11}}\frac{\partial G_1}{\partial x_1}+\frac{\partial M_{12}}{\partial c_{11}}\frac{\partial G_1}{\partial x_2} \\
&\quad+\frac{\partial M_{13}}{\partial c_{11}}\frac{\partial G_1}{\partial x_3}+\frac{\partial M_{22}}{\partial c_{11}}\frac{\partial G_2}{\partial x_2}+\frac{\partial M_{23}}{\partial c_{11}}\frac{\partial G_2}{\partial x_3}+\frac{\partial M_{33}}{\partial c_{11}}\frac{\partial G_3}{\partial x_3}dt, \\
K_{c_{13}} &= -\sum_{s=1}^{S}\sum_{r=1}^{R}\int\sum_{ijkl}\frac{\partial u_i}{\partial x_j}\frac{\partial G_k}{\partial x_l}\frac{\partial c_{ijkl}}{\partial c_{13}}dt = -\sum_{s=1}^{S}\sum_{r=1}^{R}\int\frac{\partial M_{11}}{\partial c_{13}}\frac{\partial G_1}{\partial x_1}+\frac{\partial M_{12}}{\partial c_{13}}\frac{\partial G_1}{\partial x_2} \\
&\quad+\frac{\partial M_{13}}{\partial c_{13}}\frac{\partial G_1}{\partial x_3}+\frac{\partial M_{22}}{\partial c_{13}}\frac{\partial G_2}{\partial x_2}+\frac{\partial M_{23}}{\partial c_{13}}\frac{\partial G_2}{\partial x_3}+\frac{\partial M_{33}}{\partial c_{13}}\frac{\partial G_3}{\partial x_3}dt, \\
K_{c_{33}} &= -\sum_{s=1}^{S}\sum_{r=1}^{R}\int\sum_{ijkl}\frac{\partial u_i}{\partial x_j}\frac{\partial G_k}{\partial x_l}\frac{\partial c_{ijkl}}{\partial c_{33}}dt = -\sum_{s=1}^{S}\sum_{r=1}^{R}\int\frac{\partial M_{11}}{\partial c_{33}}\frac{\partial G_1}{\partial x_1}+\frac{\partial M_{12}}{\partial c_{33}}\frac{\partial G_1}{\partial x_2} \\
&\quad+\frac{\partial M_{13}}{\partial c_{33}}\frac{\partial G_1}{\partial x_3}+\frac{\partial M_{22}}{\partial c_{33}}\frac{\partial G_2}{\partial x_2}+\frac{\partial M_{23}}{\partial c_{33}}\frac{\partial G_2}{\partial x_3}+\frac{\partial M_{33}}{\partial c_{33}}\frac{\partial G_3}{\partial x_3}dt, \\
K_{c_{44}} &= -\sum_{s=1}^{S}\sum_{r=1}^{R}\int\sum_{ijkl}\frac{\partial u_i}{\partial x_j}\frac{\partial G_k}{\partial x_l}\frac{\partial c_{ijkl}}{\partial c_{44}}dt = -\sum_{s=1}^{S}\sum_{r=1}^{R}\int\frac{\partial M_{11}}{\partial c_{44}}\frac{\partial G_1}{\partial x_1}+\frac{\partial M_{12}}{\partial c_{44}}\frac{\partial G_1}{\partial x_2} \\
&\quad+\frac{\partial M_{13}}{\partial c_{44}}\frac{\partial G_1}{\partial x_3}+\frac{\partial M_{22}}{\partial c_{44}}\frac{\partial G_2}{\partial x_2}+\frac{\partial M_{23}}{\partial c_{44}}\frac{\partial G_2}{\partial x_3}+\frac{\partial M_{33}}{\partial c_{44}}\frac{\partial G_3}{\partial x_3}dt, \\
K_{c_{66}} &= -\sum_{s=1}^{S}\sum_{r=1}^{R}\int\sum_{ijkl}\frac{\partial u_i}{\partial x_j}\frac{\partial G_k}{\partial x_l}\frac{\partial c_{ijkl}}{\partial c_{66}}dt = -\sum_{s=1}^{S}\sum_{r=1}^{R}\int\frac{\partial M_{11}}{\partial c_{66}}\frac{\partial G_1}{\partial x_1}+\frac{\partial M_{12}}{\partial c_{66}}\frac{\partial G_1}{\partial x_2} \\
&\quad+\frac{\partial M_{13}}{\partial c_{66}}\frac{\partial G_1}{\partial x_3}+\frac{\partial M_{22}}{\partial c_{66}}\frac{\partial G_2}{\partial x_2}+\frac{\partial M_{23}}{\partial c_{66}}\frac{\partial G_2}{\partial x_3}+\frac{\partial M_{33}}{\partial c_{66}}\frac{\partial G_3}{\partial x_3}dt, \\
K_{\theta} &= -\sum_{s=1}^{S}\sum_{r=1}^{R}\int\sum_{ijkl}\frac{\partial u_i}{\partial x_j}\frac{\partial G_k}{\partial x_l}\frac{\partial c_{ijkl}}{\partial \theta}dt = -\sum_{s=1}^{S}\sum_{r=1}^{R}\int\frac{\partial M_{11}}{\partial \theta}\frac{\partial G_1}{\partial x_1}+\frac{\partial M_{12}}{\partial \theta}\frac{\partial G_1}{\partial x_2} \\
&\quad+\frac{\partial M_{13}}{\partial \theta}\frac{\partial G_1}{\partial x_3}+\frac{\partial M_{22}}{\partial \theta}\frac{\partial G_2}{\partial x_2}+\frac{\partial M_{23}}{\partial \theta}\frac{\partial G_2}{\partial x_3}+\frac{\partial M_{33}}{\partial \theta}\frac{\partial G_3}{\partial x_3}dt,
\end{aligned}
\tag{15}
$$

where, M_{ij} is the moment tensor in TTI media as

$$
M_{ij} = c'_{ijkl}\epsilon'_{kl}, \tag{16}
$$

in which, c'_{ijkl} can be determined by equation (13), ϵ'_{kl} denotes the strain tensor in TTI media.

Each term of equation (15) can be determined according to equation (14) and equation

(16), which is shown in Appendix.

Alternatively, the gradients of Thomsen parameters can also be obtained based on equation (8) as

$$
\begin{aligned}
K_{V_{P0}} &= \sum_{ijkl} K_{c_{ijkl}} \frac{\partial c_{ijkl}}{\partial V_{P0}} = K_{c_{11}} \frac{\partial c_{11}}{\partial V_{P0}} + K_{c_{13}} \frac{\partial c_{13}}{\partial V_{P0}} + K_{c_{33}} \frac{\partial c_{33}}{\partial V_{P0}} + K_{c_{44}} \frac{\partial c_{44}}{\partial V_{P0}} + K_{c_{66}} \frac{\partial c_{66}}{\partial V_{P0}}, \\
K_{V_{S0}} &= \sum_{ijkl} K_{c_{ijkl}} \frac{\partial c_{ijkl}}{\partial V_{S0}} = K_{c_{11}} \frac{\partial c_{11}}{\partial V_{S0}} + K_{c_{13}} \frac{\partial c_{13}}{\partial V_{S0}} + K_{c_{33}} \frac{\partial c_{33}}{\partial V_{S0}} + K_{c_{44}} \frac{\partial c_{44}}{\partial V_{S0}} + K_{c_{66}} \frac{\partial c_{66}}{\partial V_{S0}}, \\
K_{\varepsilon} &= \sum_{ijkl} K_{c_{ijkl}} \frac{\partial c_{ijkl}}{\partial \varepsilon} = K_{c_{11}} \frac{\partial c_{11}}{\partial \varepsilon} + K_{c_{13}} \frac{\partial c_{13}}{\partial \varepsilon} + K_{c_{33}} \frac{\partial c_{33}}{\partial \varepsilon} + K_{c_{44}} \frac{\partial c_{44}}{\partial \varepsilon} + K_{c_{66}} \frac{\partial c_{66}}{\partial \varepsilon}, \\
K_{\delta^*} &= \sum_{ijkl} K_{c_{ijkl}} \frac{\partial c_{ijkl}}{\partial \delta^*} = K_{c_{11}} \frac{\partial c_{11}}{\partial \delta^*} + K_{c_{13}} \frac{\partial c_{13}}{\partial \delta^*} + K_{c_{33}} \frac{\partial c_{33}}{\partial \delta^*} + K_{c_{44}} \frac{\partial c_{44}}{\partial \delta^*} + K_{c_{66}} \frac{\partial c_{66}}{\partial \delta^*}, \\
K_{\gamma} &= \sum_{ijkl} K_{c_{ijkl}} \frac{\partial c_{ijkl}}{\partial \gamma} = K_{c_{11}} \frac{\partial c_{11}}{\partial \gamma} + K_{c_{13}} \frac{\partial c_{13}}{\partial \gamma} + K_{c_{33}} \frac{\partial c_{33}}{\partial \gamma} + K_{c_{44}} \frac{\partial c_{44}}{\partial \gamma} + K_{c_{66}} \frac{\partial c_{66}}{\partial \gamma}.
\end{aligned}
\tag{17}
$$

Each term of equation (17) can be determined, which is shown in Appendix.

INVERSE PROBLEM AND GRADIENT CALCULATION

Gradients calculation of Gaussian anomaly model

First of all, a simple Gaussian anomaly model is used to test the gradient computation based on the gradient equations in TTI media. The model is shown in Figure (1), where, the red dot denotes the source. The Gaussian anomaly lies in the middle of the model, and a total number of 48*48 receivers are evenly spaced in the yellow plane. The 3-component residual data can be acquired by calculating the difference between the observed data in the presence of Gaussian anomaly and the background modeled data with a homogeneous isotropic medium, shown in Figure (2)

The gradients with respect to the model elastic moduli are calculated based on equation (15), shown in Figure (8). The huge difference of the order of magnitudes between the tilt angle and the elastic moduli leads to the huge difference between their gradients (This introduces another problem, that is, how to choose a suitable step length during the update of the model or is it necessary to choose different step length parameters for parameters with different orders of magnitude. We will not discuss this issue in this paper). Based on the relationships shown in equation (8), the gradients of the misfit function with respect to Thomsen parameters can also be acquired according to equation (17), shown in Figure (9). The gradient of vertical P-wave velocity is only dependent on the elastic modulus c_{33} according to equation (7). Similarly, the vertical velocity V_{S0} is only dependent on the

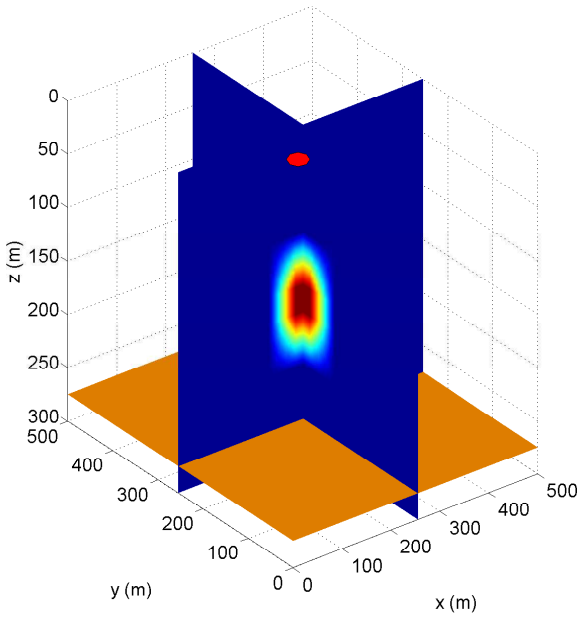

FIG. 1. Gaussian anomaly model in 3D media.

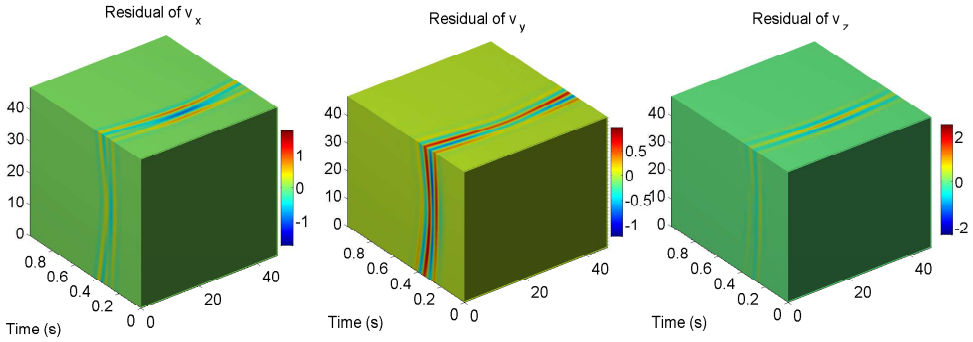

FIG. 2. 3-C residuals of Gaussian anomaly model in 3D media.

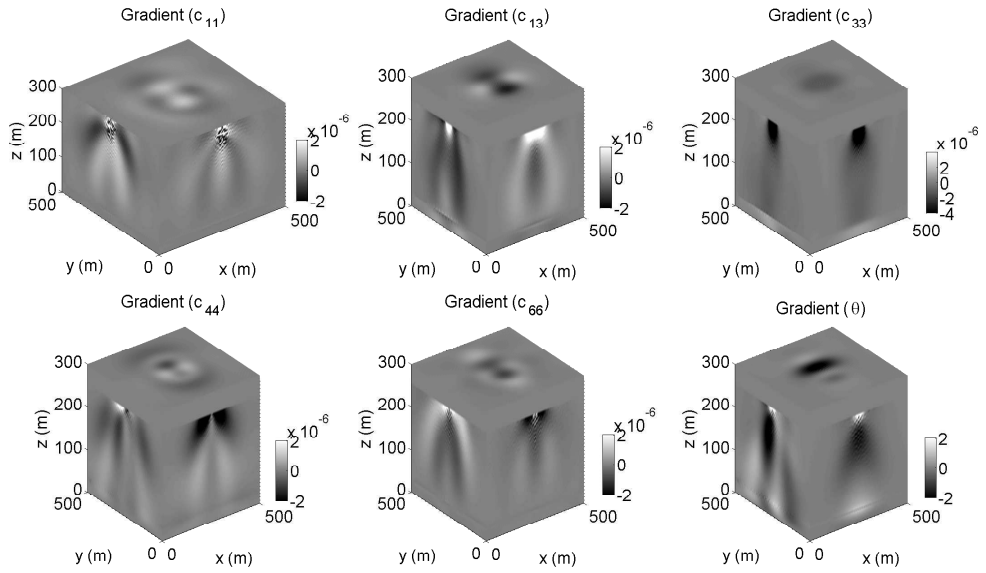

FIG. 3. Gradients of misfit function with respect to constitutive elastic moduli and tilt angle.

elastic modulus c_{44} when tilt angle equals to zero.

Gradients calculation of three-layered TTI media

In this section, a simple synthetic model will be used to calculate the gradients of misfit function. The model is a three-layer anisotropic model with different elastic moduli for each layer, whose cross-sectional is shown in Figure (5), in which the upper formation is an isotropic layer with VP, VS and density of 3500 m/s, 2000 m/s and 2500 kg/m^3. Figure (6) shows the acquisition survey in XOY plane. The right picture of Figure (5) is the initial model. The positions of sources and receivers are denoted by red circles and blue stars. 72 sources at a depth of 25 m are excited simultaneously. The evenly spaced receiver arrays (the total number of receivers is 2304) are arranged within the same depth of the source. The 3-component residual data (adjoint source) can be acquired by calculating the difference between the observed data in the presence of TTI layers and the background modeled data with a homogeneous isotropic medium (the first layer in Table (2)), shown in Figure (7). The gradients with respect to the model elastic moduli are calculated based on equation (15), shown in Figure (8). Based on the relationships shown in equation (8), the gradients of the misfit function with respect to Thomsen parameters can also be acquired according to equation (17), shown in Figure (9).

Table 2. The elastic moduli of each layer for 3D layered model.

	First layer	Second layer	Third layer	Fourth layer
c_{11}	30.6	16.2	20.1	34.9
c_{12}	10.625	8	13.95	15.75

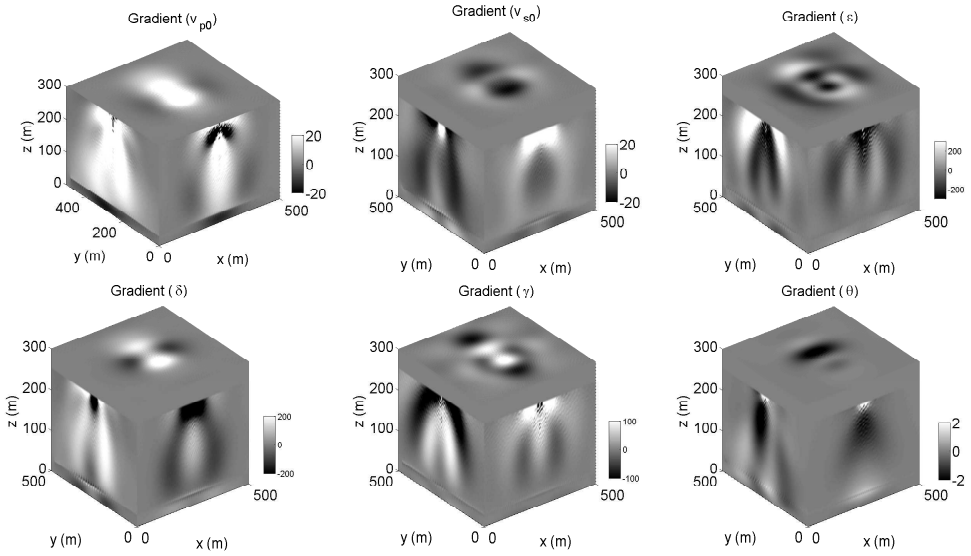

FIG. 4. Gradients of misfit function with respect to constitutive Thomsen parameters and tilt angle.

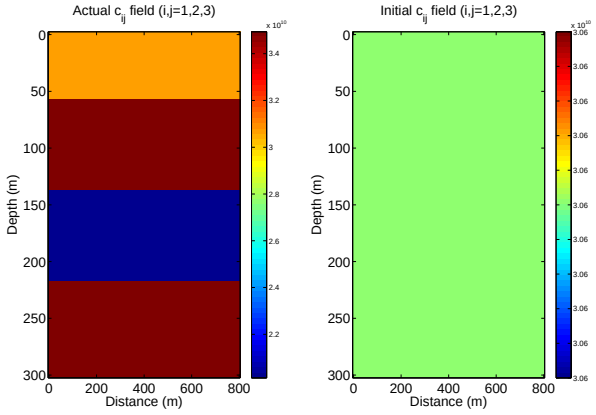

FIG. 5. Cross-section of three-layered anisotropic model and its corresponding initial model.

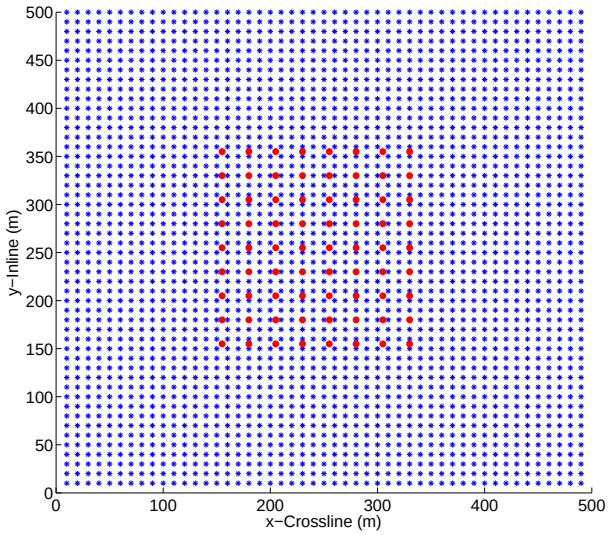

FIG. 6. The source receiver distribution geometry of the three-layered model. The red dots are the simultaneous sources and the blue stars are the distribution of receivers

	First layer	Second layer	Third layer	Fourth layer
c_{13}	10.625	5.2	11.39	12.81
c_{22}	30.6	18	23.87	40
c_{23}	10.625	8	11.18	21.25
c_{33}	30.6	16.2	15.86	38.4
c_{44}	10	4.85	3.145	9
c_{55}	10	4.3	4.371	11.81
c_{66}	10	4.85	3.895	11
c_{15}	0	1.5	2.77	1.62
c_{25}	0	1.6	2.40	4.76
c_{35}	0	1.5	0.925	1.41
c_{46}	0	0.65	0.650	-1.73

DISCUSSION

Random boundary condition

As is discussed in this paper, the staggered-grid finite difference method in time domain is applied in the synthetic wavefield forward simulation as well as the residual data time reversing propagation. The synthetic data at each time step should be stored on the disk so as to perform cross-correlation with the adjoint wavefields to generate the gradient for FWI in time domian. The huge dataset storage during synthetic wavefield simulation and loading when calculating the gradient is highly memory cost and time consuming. Symes (2007) and Anderson et al. (2012) used an optimal checkpointing algorithm to minimize the total storage at the cost of increasing the computational complexity of the adjoint wavefield

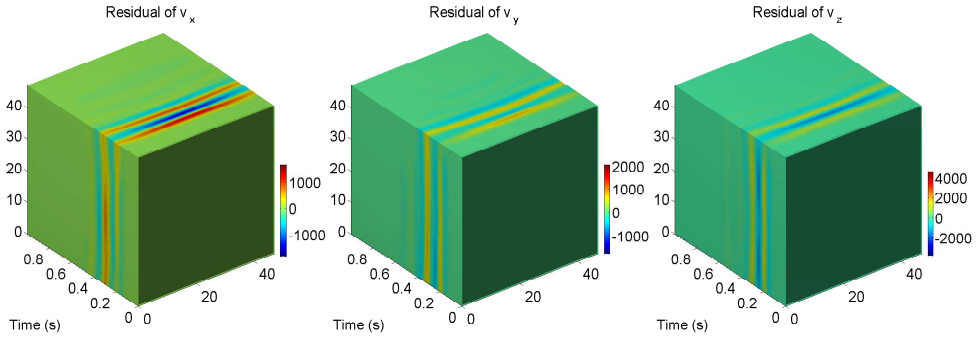

FIG. 7. The residual data for the three component velocity field.

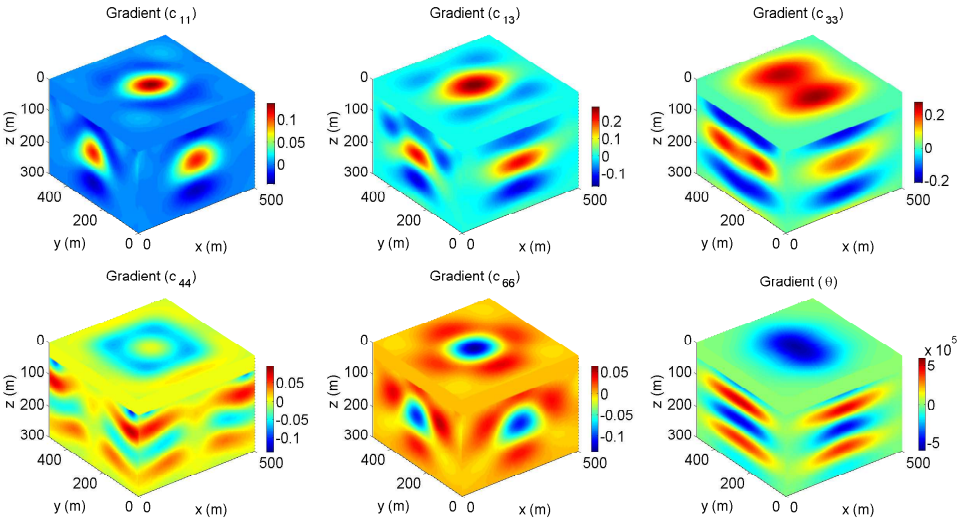

FIG. 8. Gradients of the objective function with respect to five elastic moduli and tilt angle.

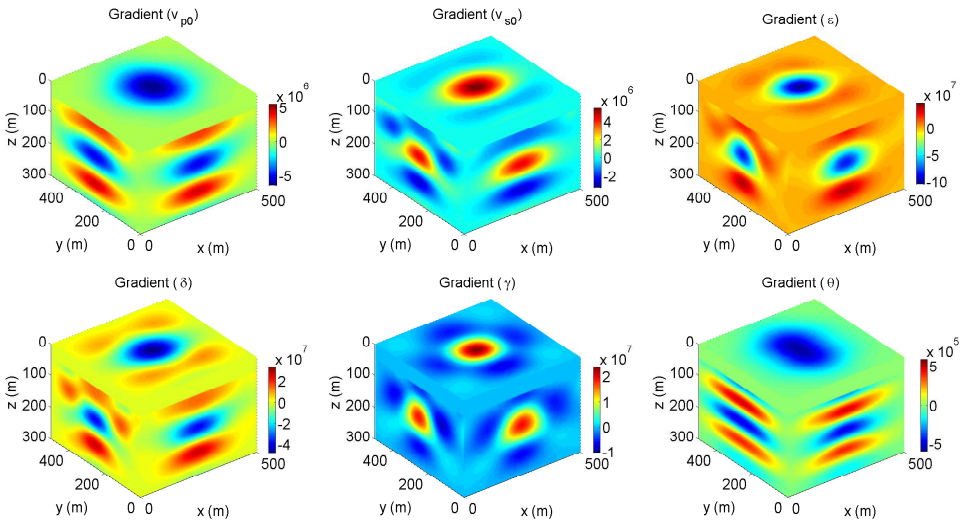

FIG. 9. Gradients of the objective function with respect to Thomsen parameters and tilt angle.

simulation. Clapp (Clapp, 2008) suggested implementing a boundary re-injection scheme that the wavefield at each time step is saved at the edge of damping zone so as to regenerate the wavefield by taking advantage of the reversibility of the wave equation. One issue of this technique is the need of injecting energy from the non-damped forward wavefield because of the conventional damped region requires significant disk IO.

Clapp et al. (2009) proposes an alternative random boundary condition method that uses an increasingly random velocity region by replacing the conventional damped region. The principle of this new scheme is to distort the reflections outside the computational areas rather than eliminate them so as to minimize coherent correlations with the adjoint wavefield while preserving the reversibility of wave equation. This allows us to compute both the adjoint and synthetic wavefield simultaneously without the necessity of storing total synthetic data. Shen and Clapp (2015) applied the random boundary condition into gradient calculation for FWI, in which larger irregularly shaped zones of randomized velocities are used to introduce incoherency in wavefronts at a large range of wavelengths. In this paper, cubic grains with 5 m side length (the same as the FD space interval) are implemented as random boundary layers. The randomized elastic moduli instead of velocities are thus added in elastic wave equations in TTI medium.

Figure 10 (Left) shows the random parameter cubic grains with 5 m side length outside the computational areas. Instead of adding a random term that relates to the distance within boundary(Clapp et al., 2009), an exponential attenuation term r is multiplied with the elastic moduli to guarantee no boundary reflections are generated in random layers. The attenuation term r can be described as

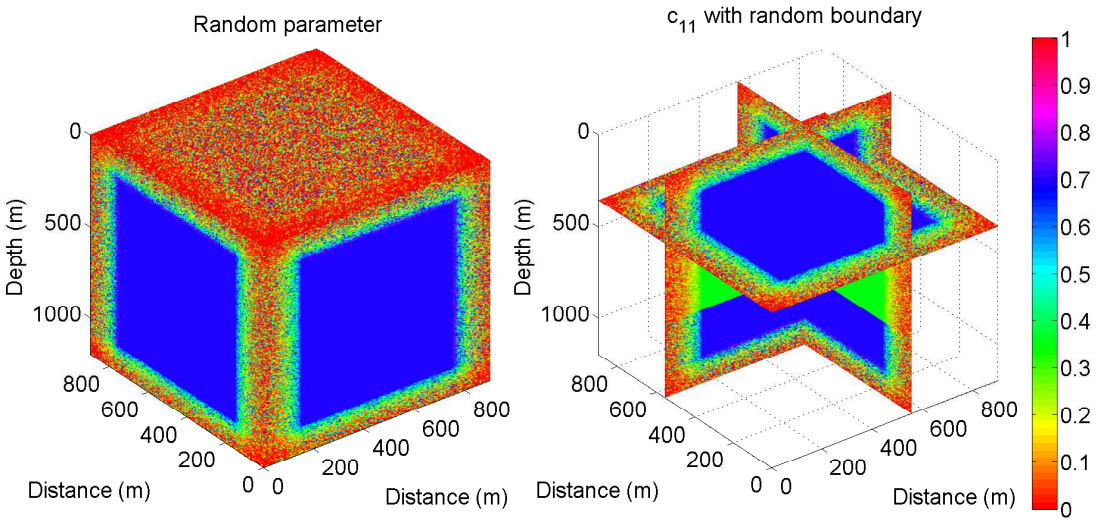

FIG. 10. Random parameter in 3D volume (Left) and randomized normal stress component τ_{xx}.

$$r = \left(rand \cdot \frac{d}{AB} \right)^n, \tag{18}$$

where, rand denotes random number within the interval of [0,1]; AB is the number of boundary layers ($AB = 30$ in this paper); d is the distance within boundary and n is the attenuation index. In isotropic media, the index can be set as $n = 1$ if velocities are subject to the exponential attenuation term. In this paper, the index can be set as $5 >= n >= 3$ when elastic moduli are subject to the exponential attenuation term.

Figure 10 (Right) shows the elastic modulus c_{11} in a three-layer model when the random boundary layers are applied (n=4). The randomized elastic moduli are thus used in synthetic data forward simulation in FWI.

Figure 11 shows the wavefield propagation (normal stress component τ_{xx}) in the synthetic model from 0.15 s to 0.3 s. The central frequency of the point source used in this example is 30 Hz. With the increasing of propagation time, the wavefield travels from the source into the random boundary where all boundary reflections generated along and inside the random layers are distorted because of the randomly distributed elastic moduli, these distorted boundary reflections are treated as noise which show low coherence with the time reversed adjoint wavefield during gradients calculation.

Figure 12 and 13 show snapshots in both xy- and xz- plane, respectively, with travel

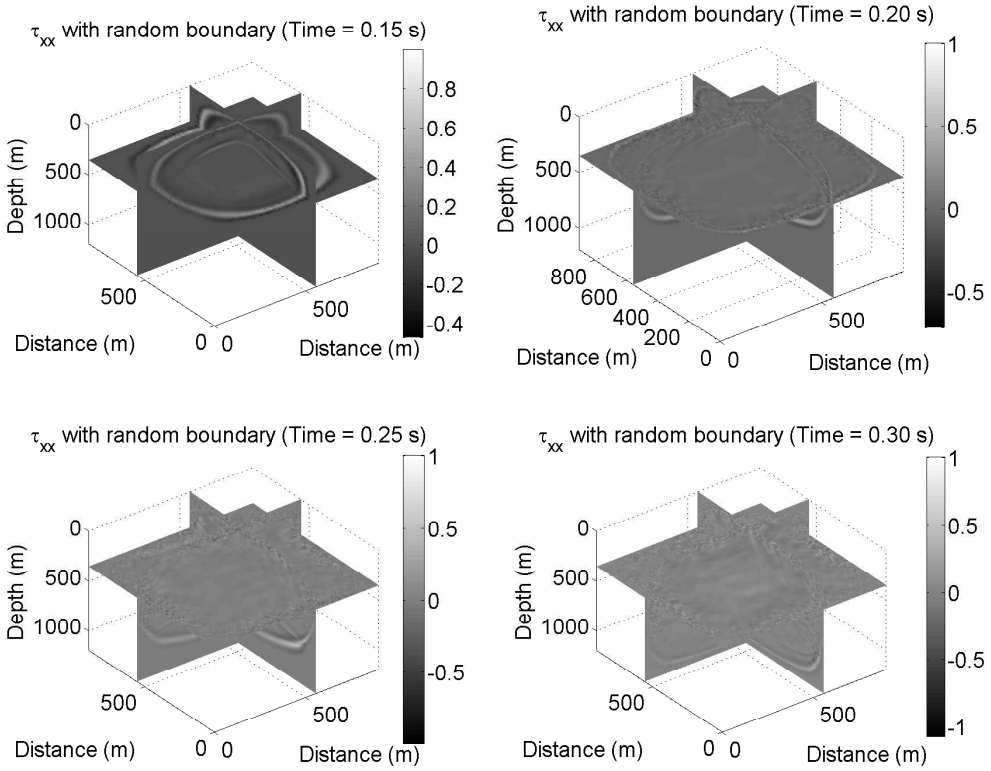

FIG. 11. τ_{xx} wavefield propagation with random boundary layers

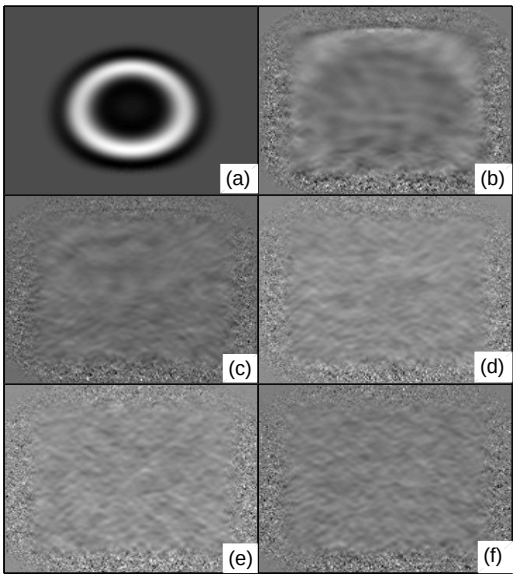

FIG. 12. Snapshots in xy-plane with travel time ranging from 0.15 s to 0.9 s

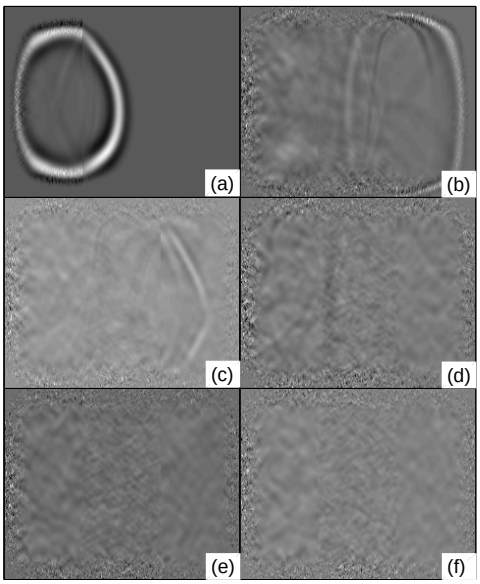

FIG. 13. Snapshots in xz-plane with travel time ranging from 0.15 s to 0.9 s

time ranging from 0.15 s to 0.9 s. The snapshots in xy-plane show the current random boundary has distorted reflections from the computational boundaries. The snapshots in xz-plane show that the randomized boundary reflections act as random background noise (13 (b) and (c)) when true reflections travel through computational areas. Theoretically, these random background noise will scatter coherent wavefields effectively and thus the adjoint wavefield time reversing simulation can be performed simultaneously with the synthetic model backward simulation, which in turn makes it possible to calculate coherence parameter or gradient of each model parameter perturbation at each time step.

CONCLUSIONS

When performing FWI, one of the most important steps is the gradient calculation of the objective function with respect to the model parameters. In 3-D TTI medium, the model can be characterized by the constitutive elastic moduli, density, tilt angle as well as the phase angle. In this paper, we discussed gradient computation in regard to both the elastic moduli and Thomsen parameters for elastic multicomponent wavefields from 3D TTI media.

Based on the adjoint state method, the synthetic and adjoint wavefields are simulated with a staggered-grid finite-difference algorithm in anisotropic media. Numerical examples of the gradients calculation in a medium with the presence of Gaussian anomaly media as well as in the three-layered anisotropic media are illustrated.

One of the issues addressed in the discussion is that the synthetic data at each time step

should be stored on the disk so as to perform cross-correlation with the adjoint wavefields to generate the gradient for FWI in time domian. The huge dataset storage during synthetic wavefield simulation and loading when calculating the gradient is highly memory cost and time consuming. In this paper, the random boundary layer is used to compute both the adjoint and synthetic wavefield simultaneously without the necessity of storing total synthetic data. The randomized elastic moduli instead of velocities are thus added in elastic wave equations in TTI medium. The synthetic waveforms with random boundary layers are finally illustrated.

For further study, the random boundary layer in regard to the elastic moduli should be implemented into the adjoint state method so as to efficiently calculate the gradient of misfit function without a huge burden of I/O on the disk as well as high memory cost. An appropriate line-search technique should also be used so as to update the model for FWI.

ACKNOWLEDGMENTS

This research was supported by the Consortium for Research in Elastic Wave Exploration Seismology (CREWES) and National Science and Engineering Research Council of Canada (NSERC, CRDPJ 379744-08). The first author also thanks to the supporting by SEG and CSEG scholarship.

APPENDIX: DERIVATIVES OF MOMENT TENSOR AND ELASTIC MODULI

According to equation (16) and (14), the derivative of moment M_{ij} tensor with respect to constitutive elastic moduli and tilt angle can be described as

$$
\begin{aligned}
\frac{\partial M_{11}}{\partial c_{11}} &= \frac{\partial u_x}{\partial x} cos^4\theta + \frac{\partial u_y}{\partial y} cos^2\theta + \frac{\partial u_z}{\partial z}\frac{sin^2(2\theta)}{4} + (\frac{\partial u_x}{\partial z} + \frac{\partial u_z}{\partial x}) cos^3\theta sin\theta \\
\frac{\partial M_{11}}{\partial c_{13}} &= \frac{\partial u_x}{\partial x}\frac{sin^2 2\theta}{2} + \frac{\partial u_y}{\partial y} sin^2\theta + \frac{\partial u_z}{\partial z}(cos^4\theta + sin^4\theta) + (\frac{\partial u_x}{\partial z} + \frac{\partial u_z}{\partial x})\frac{sin^4\theta}{4} \\
\frac{\partial M_{11}}{\partial c_{33}} &= \frac{\partial u_x}{\partial x} sin^4\theta + \frac{\partial u_z}{\partial z}(cos^2\theta sin^2\theta) + (\frac{\partial u_x}{\partial z} + \frac{\partial u_z}{\partial x})\left(-sin^3\theta cos\theta\right) \\
\frac{\partial M_{11}}{\partial c_{44}} &= \frac{\partial u_x}{\partial x} sin^2(2\theta) + \frac{\partial u_z}{\partial z}(-sin^2(2\theta)) + (\frac{\partial u_x}{\partial z} + \frac{\partial u_z}{\partial x})\left(sin2\theta cos2\theta\right) \\
\frac{\partial M_{11}}{\partial c_{66}} &= -2cos^2\theta\frac{\partial u_y}{\partial y} \\
\frac{\partial M_{12}}{\partial c_{11}} &= \frac{\partial u_x}{\partial x} cos^2\theta + \frac{\partial u_y}{\partial y} + \frac{\partial u_z}{\partial z}\frac{sin^2(\theta)}{4} + (\frac{\partial u_x}{\partial z} + \frac{\partial u_z}{\partial x})\left(-\frac{1}{2}sin2\theta\right) \\
\frac{\partial M_{12}}{\partial c_{13}} &= \frac{\partial M_{12}}{\partial c_{33}} = 0 \\
\frac{\partial M_{12}}{\partial c_{44}} &= (\frac{\partial u_y}{\partial z} + \frac{\partial u_z}{\partial y})\left(-sin\theta cos\theta\right) + (\frac{\partial u_x}{\partial y} + \frac{\partial u_y}{\partial x}) sin^2\theta \\
\frac{\partial M_{12}}{\partial c_{66}} &= cos^2\theta(\frac{\partial u_x}{\partial y} + \frac{\partial u_y}{\partial x}) + sin\theta cos\theta(\frac{\partial u_y}{\partial z} + \frac{\partial u_z}{\partial y}) \\
\frac{\partial M_{13}}{\partial c_{11}} &= \frac{\partial u_x}{\partial x} cos^3\theta sin\theta + \frac{\partial u_z}{\partial z} sin^3(\theta) cos\theta + (\frac{\partial u_x}{\partial z} + \frac{\partial u_z}{\partial x})\left(sin2\theta cos^2\theta\right) \\
\frac{\partial M_{13}}{\partial c_{13}} &= \frac{\partial u_x}{\partial x}\left(-cos^3\theta sin\theta + sin^3\theta cos\theta\right) + \frac{\partial u_y}{\partial y}\left(-sin\theta cos\theta\right) \\
&\quad + \frac{\partial u_z}{\partial z}\left(-sin^3(\theta) cos\theta + cos^3(\theta) sin\theta\right) + (\frac{\partial u_x}{\partial z} + \frac{\partial u_z}{\partial x})\left(sin2\theta cos^2\theta\right) \\
\frac{\partial M_{13}}{\partial c_{33}} &= \frac{\partial u_x}{\partial x}\left(-sin^3\theta cos\theta\right) + \frac{\partial u_z}{\partial z}\left(cos^2(\theta) sin\theta\right) + \frac{1}{4} sin^2(2\theta) \\
\frac{\partial M_{13}}{\partial c_{44}} &= \frac{\partial u_x}{\partial x}\left(-sin2\theta cos2\theta\right) + \frac{\partial u_z}{\partial z} sin2\theta cos2\theta + (\frac{\partial u_x}{\partial z} + \frac{\partial u_z}{\partial x}) cos^2(2\theta)
\end{aligned}
\tag{19}
$$

and

$$\frac{\partial M_{13}}{\partial c_{66}} = -sin2\theta\frac{\partial u_y}{\partial y}$$

$$\frac{\partial M_{22}}{\partial c_{11}} = \frac{\partial u_x}{\partial x}cos^2\theta + \frac{\partial u_y}{\partial y}cos^4\theta + \frac{\partial u_z}{\partial z}\frac{sin^2(2\theta)}{4} + (\frac{\partial u_x}{\partial z} + \frac{\partial u_z}{\partial x})cos^3\theta sin\theta$$

$$\frac{\partial M_{22}}{\partial c_{13}} = \frac{\partial u_x}{\partial x}sin^2\theta + \frac{\partial u_z}{\partial z}cos^2\theta + (\frac{\partial u_x}{\partial z} + \frac{\partial u_z}{\partial x})cos\theta sin\theta$$

$$\frac{\partial M_{22}}{\partial c_{33}} = \frac{\partial u_z}{\partial z}cos^4\theta, \quad \frac{\partial M_{22}}{\partial c_{44}} = 0$$

$$\frac{\partial M_{22}}{\partial c_{66}} = -2cos^2\theta\frac{\partial u_x}{\partial x} - 2sin^2\theta\frac{\partial u_z}{\partial z} - 2cos\theta sin\theta(\frac{\partial u_x}{\partial z} + \frac{\partial u_z}{\partial x})$$

$$\frac{\partial M_{23}}{\partial c_{11}} = \frac{\partial M_{23}}{\partial c_{13}} = \frac{\partial M_{23}}{\partial c_{33}} = 0$$

$$\frac{\partial M_{23}}{\partial c_{44}} = cos^2\theta(\frac{\partial u_y}{\partial z} + \frac{\partial u_z}{\partial y}) + (-sin\theta cos\theta)\left(\frac{\partial u_x}{\partial y} + \frac{\partial u_y}{\partial x}\right) \tag{20}$$

$$\frac{\partial M_{33}}{\partial c_{11}} = \frac{\partial u_x}{\partial x}\frac{sin^2 2\theta}{4} + \frac{\partial u_y}{\partial y}sin^2\theta + \frac{\partial u_z}{\partial z}sin^4\theta + (\frac{\partial u_x}{\partial z} + \frac{\partial u_z}{\partial x})sin^3\theta cos\theta$$

$$\begin{aligned}\frac{\partial M_{33}}{\partial c_{13}} = &\frac{\partial u_x}{\partial x}\left(cos^4\theta + sin^4\theta\right) + \frac{\partial u_y}{\partial y}sin^2\theta + \frac{1}{2}\frac{\partial u_z}{\partial z}sin^2 2\theta \\ &+ (\frac{\partial u_x}{\partial z} + \frac{\partial u_z}{\partial x})\left(cos^3\theta sin\theta - sin^3\theta cos\theta\right)\end{aligned}$$

$$\frac{\partial M_{33}}{\partial c_{33}} = \frac{\partial u_x}{\partial x}\frac{sin^2(2\theta)}{4} + \frac{\partial u_z}{\partial z}cos^4\theta + (\frac{\partial u_x}{\partial z} + \frac{\partial u_z}{\partial x})\left(-cos^3\theta sin\theta\right)$$

$$\frac{\partial M_{33}}{\partial c_{44}} = \frac{\partial u_x}{\partial x}\left(-sin^2(2\theta)\right) + \frac{\partial u_z}{\partial z}sin^2(2\theta) + (\frac{\partial u_x}{\partial z} + \frac{\partial u_z}{\partial x})\left(cos2\theta sin2\theta\right)$$

$$\frac{\partial M_{33}}{\partial c_{66}} = -2sin^2\theta\frac{\partial u_y}{\partial y}$$

and,

$$\begin{aligned}
\frac{\partial M_{11}}{\partial \theta} &= \left[2sin2\theta\left(c_{33}sin^2\theta - c_{11}cos^2\theta\right) - \left(c_{13+2c_{44}}\right)sin4\theta\right]\frac{\partial u_x}{\partial x} \\
&+ \left[sin2\theta\left(c_{13} - c11 + 2c_{66}\right)\right]\frac{\partial u_y}{\partial y} + \left[sin4\theta\left(\frac{1}{2}\left(c_{11} + c33 - 4c_{44}\right) - c_{13}\right)\right]\frac{\partial u_z}{\partial z} \\
&+ \left[(c_{11} - c_{13})(cos^4\theta - 3cos^2\theta sin^2\theta)\right]\left(\frac{\partial u_x}{\partial z} + \frac{\partial u_z}{\partial x}\right) \\
&+ \left[(c_{15} - c_{33})(3sin^2\theta cos^2\theta - sin^4\theta) - 2c_{44}(cos^2 2\theta - sin^2 2\theta)\right]\left(\frac{\partial u_x}{\partial z} + \frac{\partial u_z}{\partial x}\right)
\end{aligned}$$

$$\frac{\partial M_{12}}{\partial \theta} = (c_{66} - c_{44})cos2\theta\left(\frac{\partial u_y}{\partial z} + \frac{\partial u_z}{\partial y}\right) + \left(c_{44} - c_{66}\right)sin2\theta\left(\frac{\partial u_x}{\partial z} + \frac{\partial u_z}{\partial x}\right)$$

$$\begin{aligned}
\frac{\partial M_{13}}{\partial \theta} &= \left[(c_{11} - c_{13})(cos^4\theta - 3cos^2\theta sin^2\theta) + (c_{15} - c_{33})(3sin^2\theta cos^2\theta - sin^4\theta)\right]\frac{\partial u_x}{\partial x} \\
&- 2c_{44}cos4\theta\frac{\partial u_x}{\partial x} + cos(2\theta)\left(c_{11} - 2c_{66} - c_{13}\right)\frac{\partial u_y}{\partial y} + 2c_{44}cos4\theta\frac{\partial u_z}{\partial z} \\
&+ \left[(c_{11} - c_{13})(3sin^2\theta cos^2\theta - sin^4\theta) + (c_{13} - c_{33})(cos^4\theta - 3cos^2\theta sin^2\theta)\right]\frac{\partial u_z}{\partial z} \\
&+ sin4\theta\left[\frac{1}{2}(c_{11} - 2c_{13} + c_{33} - 2c_{44})\right]\left(\frac{\partial u_x}{\partial z} + \frac{\partial u_z}{\partial x}\right)
\end{aligned}$$

$$\frac{\partial M_{22}}{\partial \theta} = \left(c_{13} - c_{11} + 2c_{66}\right)\left[sin2\theta\left(\frac{\partial u_x}{\partial x} + \frac{\partial u_z}{\partial z}\right) + cos2\theta\left(\frac{\partial u_x}{\partial z} + \frac{\partial u_z}{\partial x}\right)\right]$$

$$\frac{\partial M_{23}}{\partial \theta} = (c_{66} - c_{44})sin2\theta\left(\frac{\partial u_y}{\partial z} + \frac{\partial u_z}{\partial y}\right) + \left(c_{66} - c_{44}\right)cos2\theta\left(\frac{\partial u_x}{\partial y} + \frac{\partial u_y}{\partial x}\right)$$

$$\begin{aligned}
\frac{\partial M_{33}}{\partial \theta} &= \left[\frac{1}{2}(c_{11} + c_{33} - c_{44}) - c_{13}\right]sin4\theta\frac{\partial u_x}{\partial x} + (c_{11} - 2c_{66} - c_{33})sin2\theta\frac{\partial u_y}{\partial y} \\
&+ \left[2sin2\theta(c_{11}sin^2\theta - c_{33}cos^2\theta) + (c_{13} + 2c_{44})sin4\theta\right]\frac{\partial u_z}{\partial z} \\
&+ \left[(c_{11} - c_{13})(3sin^2\theta cos^2\theta - sin^4\theta) + (c_{13} - c_{33})(cos^4\theta - 3cos^2\theta sin^2\theta)\right]\frac{\partial u_z}{\partial z} \\
&+ \left[(c_{11} - c_{13})(3sin^2\theta cos^2\theta - sin^4\theta) + 2c_{44}cos4\theta\right]\left(\frac{\partial u_x}{\partial z} + \frac{\partial u_z}{\partial x}\right) \\
&+ (c_{13} - c_{33})(cos^4\theta - 3cos^2\theta sin^2\theta)\left(\frac{\partial u_x}{\partial z} + \frac{\partial u_z}{\partial x}\right)
\end{aligned}$$

(21)

According to equation (8), the derivative of elastic moduli in constitutive coordinate system with respect to Thomsen parameters can be described as

$$
\begin{aligned}
&\frac{\partial c_{11}}{\partial V_{P0}} = 2\rho(2\varepsilon+1)V_{P0}, \quad \frac{\partial c_{11}}{\partial \varepsilon} = 2\rho V_{P0} \\
&\frac{\partial c_{11}}{\partial V_{S0}} = 0, \quad \frac{\partial c_{11}}{\partial \delta^*} = 0, \quad \frac{\partial c_{11}}{\partial \gamma} = 0 \\
&\frac{\partial c_{13}}{\partial V_{P0}} = \frac{\rho V_{P0}\left[2V_{P0}^2(delta^*+\varepsilon+1)-V_{S0}^2(\varepsilon+2)\right]}{\left(V_{P0}^4\delta^*+(V_{P0}^2-V_{S0}^2)\left[V_{P0}^2(1+\varepsilon)-V_{S0}^2\right]\right)^{1/2}} \\
&\frac{\partial c_{13}}{\partial V_{S0}} = \left(\frac{\left[2V_{S0}^2-V_{P0}^2(\varepsilon+2)\right]}{\left(V_{P0}^4\delta^*+(V_{P0}^2-V_{S0}^2)\left[V_{P0}^2(1+\varepsilon)-V_{S0}^2\right]\right)^{1/2}} - 2\right)\rho V_{S0} \\
&\frac{\partial c_{13}}{\partial \varepsilon} = \frac{\rho V_{P0}^2(V_{P0}^2-V_{S0}^2)}{\left(V_{P0}^4\delta^*+(V_{P0}^2-V_{S0}^2)\left[V_{P0}^2(1+\varepsilon)-V_{S0}^2\right]\right)^{1/2}} \\
&\frac{\partial c_{13}}{\partial \delta^*} = \frac{\rho V_{P0}^4}{2\left(V_{P0}^4\delta^*+(V_{P0}^2-V_{S0}^2)\left[V_{P0}^2(1+\varepsilon)-V_{S0}^2\right]\right)^{1/2}} \\
&\frac{\partial c_{33}}{\partial V_{P0}} = 2\rho V_{P0}, \quad \frac{\partial c_{33}}{\partial \varepsilon} = 0 \\
&\frac{\partial c_{33}}{\partial V_{S0}} = 0, \quad \frac{\partial c_{33}}{\partial \delta^*} = 0, \quad \frac{\partial c_{33}}{\partial \gamma} = 0 \\
&\frac{\partial c_{44}}{\partial V_{P0}} = 0, \quad \frac{\partial c_{44}}{\partial \varepsilon} = 0 \\
&\frac{\partial c_{44}}{\partial V_{S0}} = 2\rho V_{S0}, \quad \frac{\partial c_{44}}{\partial \delta^*} = 0, \quad \frac{\partial c_{44}}{\partial \gamma} = 0 \\
&\frac{\partial c_{66}}{\partial V_{P0}} = 0, \quad \frac{\partial c_{66}}{\partial \varepsilon} = 0 \\
&\frac{\partial c_{66}}{\partial V_{S0}} = 2\rho V_{S0}(2\gamma+1), \quad \frac{\partial c_{66}}{\partial \delta^*} = 0, \quad \frac{\partial c_{66}}{\partial \gamma} = 2\rho V_{S0}^2
\end{aligned}
\tag{22}
$$

Substitute the above derivatives into (17), the Thomsen gradients with respect to model parameters can be determined.

REFERENCES

Anderson, J. E., Tan, L., and Wang, D., 2012, Time-reversal checkpointing methods for rtm and fwi: Geophysics, **77**, No. 4, S93–S103.

Bansal, R., and Sen, M. K., 2008, Finite-difference modelling of s-wave splitting in anisotropic media: Geophysical Prospecting, **56**, No. 3, 293–312.

Bunks, C., Saleck, F. M., Zaleski, S., and Chavent, G., 1995, Multiscale seismic waveform inversion: Geophysics, **60**, No. 5, 1457–1473.

Clapp, R. G., 2008, Reverse time migration: saving the boundaries: Stanford Exploration Project, 137.

Clapp, R. G. et al., 2009, Reverse time migration with random boundaries, *in* 2009 SEG Annual Meeting, Society of Exploration Geophysicists.

Crase, E., Pica, A., Noble, M., McDonald, J., and Tarantola, A., 1990, Robust elastic nonlinear waveform inversion: Application to real data: Geophysics, **55**, No. 5, 527–538.

Gauthier, D., 1986, Morals by agreement: Oxford University Press on Demand.

Kamath, N., Tsvankin, I. et al., 2013, Gradient computation for elastic full-waveform inversion in 2d vti media, *in* 2013 SEG Annual Meeting, Society of Exploration Geophysicists.

Kolb, P., Canadas, G. et al., 1986, Least-squares inversion of prestack data: Simultaneous identification of density and velocity of stratified media, *in* 1986 SEG Annual Meeting, Society of Exploration Geophysicists.

Komatitsch, D., and Tromp, J., 2002, Spectral-element simulations of global seismic wave propagationâĂŤi. validation: Geophysical Journal International, **149**, No. 2, 390–412.

Lailly, P., 1983, The seismic inverse problem as a sequence of before stack migrations.

Lee, H.-Y., Koo, J. M., Min, D.-J., Kwon, B.-D., and Yoo, H. S., 2010, Frequency-domain elastic full waveform inversion for vti media: Geophysical Journal International, **183**, No. 2, 884–904.

Liu, Q., and Tromp, J., 2006, Finite-frequency kernels based on adjoint methods: Bulletin of the Seismological Society of America, **96**, No. 6, 2383–2397.

Mora, P., 1987, Nonlinear two-dimensional elastic inversion of multioffset seismic data: Geophysics, **52**, No. 9, 1211–1228.

Nguyen, B. D., and McMechan, G. A., 2014, Five ways to avoid storing source wavefield snapshots in 2d elastic prestack reverse time migration: Geophysics, **80**, No. 1, S1–S18.

Palloff, R., and Pratt, K., 1999, Building learning communities in cyberspace: San Francisco.

Shen, X., and Clapp, R. G., 2015, Random boundary condition for memory-efficient waveform inversion gradient computation: Geophysics, **80**, No. 6, R351–R359.

Symes, W. W., 2007, Reverse time migration with optimal checkpointing: Geophysics, **72**, No. 5, SM213–SM221.

Tarantola, A., 1984, Inversion of seismic reflection data in the acoustic approximation: Geophysics, **49**, No. 8, 1259–1266.

Thomsen, L., 1986, Weak elastic anisotropy: Geophysics, **51**, No. 10, 1954–1966.

Tromp, J., Tape, C., and Liu, Q., 2005, Seismic tomography, adjoint methods, time reversal and banana-doughnut kernels: Geophysical Journal International, **160**, No. 1, 195–216.

Tsvankin, I., 2012, Seismic signatures and analysis of reflection data in anisotropic media, 19: SEG Books.

Winterstein, D., 1990, Velocity anisotropy terminology for geophysicists: Geophysics, **55**, No. 8, 1070–1088.

Zhu, J., and Dorman, J., 2000, Two-dimensional, three-component wave propagation in a transversely isotropic medium with arbitrary-orientation-finite-element modeling: Geophysics, **65**, No. 3, 934–942.